In situ Generation of Intimacy in MnOx+SAPO-34 Mechanical Mixture for the Conversion of Syngas to Light Olefins

C. Coudercy, M. Prevot, P. Afanasiev, S. Loridant

In situ generation of intimacy in MnOx+SAPO-34 mechanical mixture for the conversion of syngas to light olefins

Christophe Coudercy,[a] Mathieu Prevot,[a] Pavel Afanasiev,[a] Stéphane Loridant*[a]

[a] Dr. C. Coudercy, Dr. M. Prevot, Dr. P. Afanasiev, Dr. S. Loridant

Univ Lyon, Université Claude Bernard Lyon 1, CNRS, IRCELYON, 2 Av. A. Einstein F-69626 Villeurbanne Cedex, France

E-mail: stephane.loridant@ircelyon.univ-lyon1.fr, https://www.ircelyon.univ-lyon1.fr/en/syrcel-en/card/SLO/

Supporting information for this article is given via a link at the end of the document.

Abstract: Bifunctional MnOx+SAPO-34 catalysts were evaluated for the conversion of syngas to light olefins (OXZEO process). They were prepared, either by mechanical mixing of 100 µm-scale particles agglomerates, or by mixing of ethanol suspensions, containing homogeneously distributed micrometer-scale primary particles of oxide and zeolite. The selectivity to light olefins, initially lower for the mechanical mixture, reached the value of the suspension mixture after a 14 h on-stream period. This convergence was explained from SEM images by in situ breaking of SAPO-34 agglomerates present in the mechanical mixture and dispersion of SAPO-34 crystals among MnO_x primary particles, decreasing the contact distance between the two catalytic functions. These results evidence the importance of intimacy at the micrometer scale to improve the catalytic properties in the OXZEO process.

Introduction

Light olefins ($C2^=$-$C4^=$) are key building-block chemicals presently produced worldwide in huge amounts (market exceeding 320 Mt.y-1)[1] mostly by steam cracking and Fluid Catalytic Cracking (FCC). The increasing demand and the evolution of raw materials require the development of on-purpose, less energy-intensive processes. The OXZEO (Oxide-Zeolite) process is promising because it allows the selective and stable production of light olefins from syngas combining a hydrogenation catalyst to synthesize methanol or ketene and an acidic zeolite to convert the intermediate to light olefins. Since the pioneer paper of the X. Bao' group,[2] numerous other metal oxide–zeolite combinations yielding high $C2^=$-$C4^=$ selectivity have been reported and this concept was recently reviewed.[3,4]

We previously investigated the combination of MnO_x and SAPO-34 zeolite in a mechanical mixture for the conversion of syngas to light olefins and evidenced that CH3OH is a key intermediate.[5] High selectivity to $C2^=$-$C4^=$ would require optimal proximity determined by the local concentration of methanol[6] and related both to the kinetics of formation and consumption and its diffusion from the oxide to the zeolite. Furthermore, those olefins can be hydrogenated to the corresponding alkanes on the oxide. Therefore, the intimacy between the two catalysts may significantly influence the catalytic performance: as such, random mixtures of powders are usually more efficient than arrangements of catalytic beds. For the $ZnCrO_x$-SAPO-34 and MnO_x+SAPO-34 catalytic systems, it was shown that the reaction benefits from the decrease of distance between the catalytic functions due to reduced mass transport limitation. The effect was observed for granule size decreasing down to the micrometer.[7] Mortar mixing of $ZnZrO_x$ and SSZ-13 for 10 min led to improved catalytic properties.[8] However, it was

reported that ball milling of mixtures of oxide and zeolite led to degradation of the zeolite properties.[9-13].

In this work, a mixture of MnO_x nanoparticles and SAPO-34 crystals was prepared by combining suspensions of both solids to improve intimacy at the primary grain (nanometer) scale. We assumed that if two solids are dried separately and then mixed, many agglomerates of the same type of particles would persist in the mixture. On the contrary, mixing of liquid suspensions prior to drying would ensure lesser agglomeration of the same type particles and better intimacy as it have been shown for $BaTiO_3$ preparation.[14,15]

This suspension mixture (SM) was then evaluated for the conversion of syngas to light olefins and its catalytic performances were compared with those of a mechanical mixture (MM) of dry powders MnO_x+SAPO-34. The two mixtures were characterized after calcination, activation and reaction crossing different techniques, in particular Scanning Electron Microscopy. The goal was to establish a relationship between the textural and catalytic properties.

Results and Discussion

The XRD diffractogram of MnO_x (Figure 1a) shows that it contained mostly MnO and a small amount of Mn_3O_4 as crystalline phases.

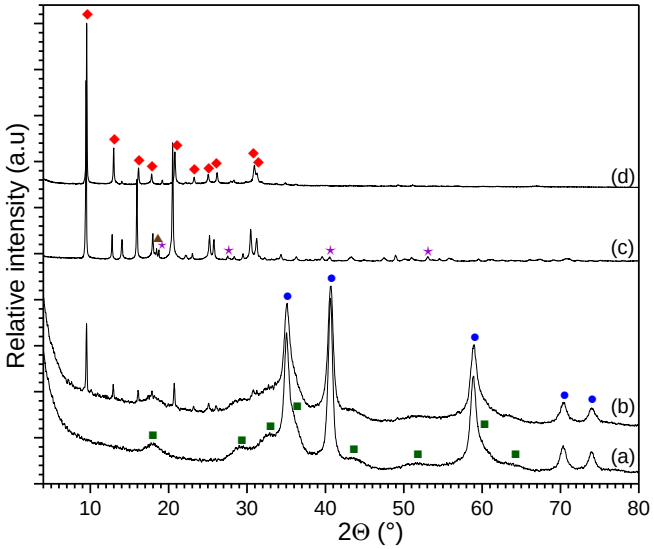

Figure 1. XRD diffractograms of (a) MnO_x and (b) 90%MnO_x+10%SAPO34-SM after thermal treatment under H_2 flow, (c) SAPO-34 after drying and (d) calcination. The diffraction peaks of (◆) SAPO-34, (●) MnO, (■) Mn_3O_4, (★) $Al(OH)_3$ Bayerite and (▲) $Al(OH)_3$ Nordstrandite were indexed with the PDF 47-0429, 75-1090, 01-1127, 74-119 and 72-0623 ICDD patterns, respectively.

This pattern revealed that $MnCO_3$ precursor was decomposed into MnO during the thermal treatment at 430 °C under 20%H_2-N_2 and then slightly oxidized upon passivation. The crystallite size of the MnO phase determined by the Scherrer equation was around 12 nm. The large width of the Mn_3O_4 peaks suggests that this phase is present as a poorly crystallized layer over MnO.

TEM images of the prepared $MnCO_3$ precursor show well defined spherical porous nanoparticles with a mean diameter of 466±44 nm (Figures 2a and b). SEM image of MnO_x (Figure 2c) shows that the morphology has been retained after thermal treatment and further reveals that the porous spheres are composed of smaller nanoparticles when the thermal treatment temperature remains below 900 °C, as reported in the literature.[16] The adsorption isotherms of the solids before and after thermal

treatment were of type V with H_2 hysteresis (Figure S1)[17-19] revealing the presence of mesoporosity in the solid. The mesopore diameter strongly increased from 8 to 24 nm upon thermal treatment (Figure S2). The BET surface area decreased after calcination from 103 to 53 $m^2.g^{-1}$.

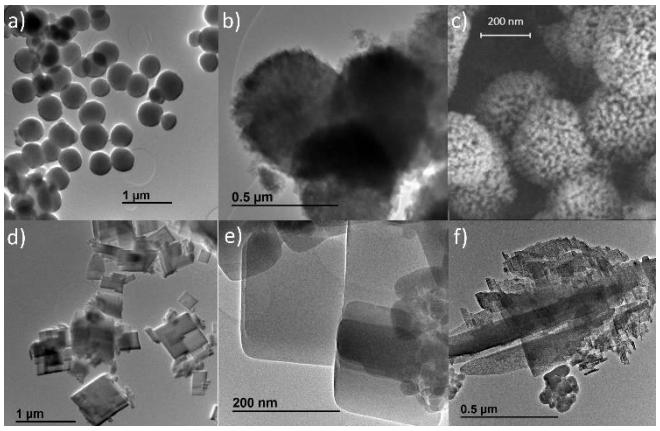

Figure 2. TEM images of a) the prepared $MnCO_3$ nanoparticles before thermal treatment. b) zoom on a single nanoparticle showing that it is porous and constituted of secondary nanoparticles c) SEM image of the prepared MnO_x nanoparticles after thermal treatment, TEM images of SAPO-34 sample showing d,e) zeolite crystals and f) extra-framework alumina.

The molar composition of SAPO-34 was Si/Al/P=0.15/1/0.68 ((Si+P)/Al=0.83). Its XRD diffractograms before and after thermal treatment (Figures 1c and d, respectively) mostly contain the peaks of the chabazite structure. They were close to the one indexed for the composition Si/Al/P:0.22/1/0.75 (PDF 47-0429 ICDD pattern). The slight shift and change of relative intensity of peaks upon thermal treatment were due to the removal of organic species during calcination, leading to slight modification of the crystalline structure.[20] However, the presence of small amounts of $Al(OH)_3$ crystalline phases was evidenced after drying (Figure 1c). The corresponding peaks were not observed after calcination suggesting that $Al(OH)_3$ was decomposed into amorphous Al_2O_3. TEM images agree with the XRD analysis since they show SAPO-34 crystals in the 100 to 300 nm size range (Figures 2d and e) as well as extra framework alumina (Figure 2f). The ^{27}Al NMR signals at 39, 10 and -12 ppm (figure S3a) were assigned to tetra, penta- and octacoordinated aluminum atoms, respectively.[21-23] The latter were formed by addition of two water molecules to tetrahedrally coordinated framework aluminum atoms or corresponded to atoms present in extra-framework Al_2O_3. The ^{31}P NMR spectrum of SAPO-34 (Figure S3b) revealed mainly a $P(OAl)_4$ local structure with a chemical shift of -27 ppm[21-23] and small amount of P(OAl)x(H2O)y hydrated local structures at -16 ppm.[22] The latter species were probably present at the outer surface of the crystals.[21,23] Only isolated Si atoms have been observed in the ^{29}Si NMR spectrum of SAPO-34, with a chemical shift of -89 ppm (Figure S3c).[21-23]

The BET surface area of the prepared SAPO-34 was 581 $m^2.g^{-1}$; that of the microporous one was 524 $m^2.g^{-1}$, the difference between the two values (57$m^2.g^{-1}$) corresponding probably to the intergranular porosity. The prepared SAPO-34 contained 894 µmol.g^{-1} of weak acidic sites and 925 µmol.g^{-1} of strong ones as probed by NH_3-TPD (Figure S4).

The suspension mixture sample 90%MnO_x+10%SAPO-34-SM was characterized by XRD after thermal treatment under 20%H_2-N_2. Its diffractogram (Figure 1b) corresponded to a combination of MnO_x (also treated under 20%H_2-N_2, Figure 1a) and SAPO-34 after calcination (Figure 1d), showing that the phase composition of SM was similar to that of the MM. SEM image of the SM sample (Figures 3a and S5) shows SAPO-34 crystals highly dispersed among the MnO_x nanoparticles. On the contrary, large aggregates (100-200 µm) of either MnO_x or SAPO-34 were observed for 90%MnO_x+10%SAPO-34-MM,

(Figures 3b and S6) with clear separation between them (Figure 3c) even if a small quantity of MnO_x nanoparticles covers SAPO-34 aggregates. Hence, as expected, the intimacy between MnO_x and SAPO-34 phases is higher for the SM sample than for the MM one.

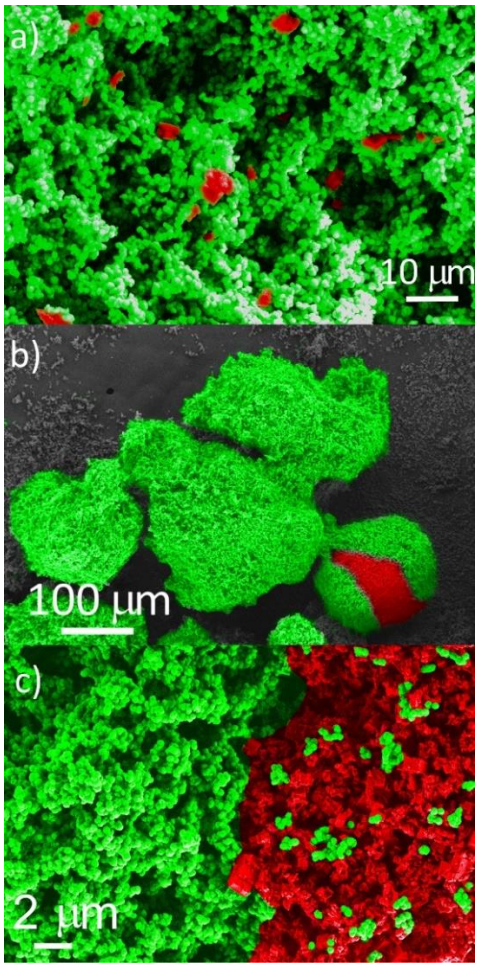

Figure 3: SEM images of a) 90%MnO_x+10%SAPO-34-SM sample after thermal treatment under H_2 flow, of b) fresh 90%MnO_x+10%SAPO-34-MM sample showing aggregates of MnO_x on the left and one of SAPO-34 in the down right corner and c) zoom of this image showing MnO_x and SAPO-34 separation. SAPO-34 crystals are colored in red and MnOx nanoparticles in green.

The catalytic properties of MnO_x+SAPO-34-MM and MnO_x+SAPO-34-SM mixtures were assessed to determine the impact of the difference of intimacy at the grain scale. Figure 4a compares the time evolution of the CO conversion: it was quite similar and close to 4% for the two mixtures.

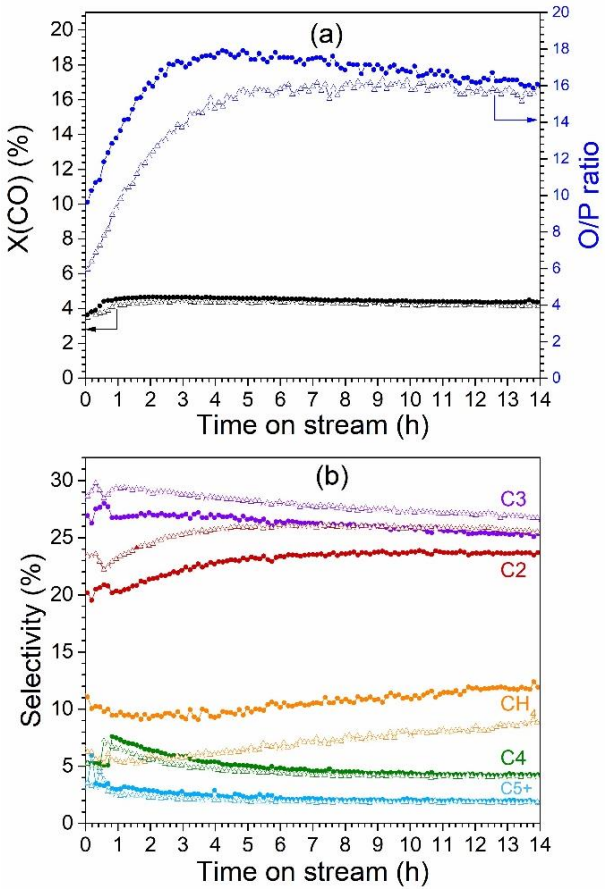

Figure 4. (a) evolution of the X(CO) conversion and O/P ratio with time on stream, (b) evolution of the hydrocarbon selectivity with time on stream for MnO_x+SAPO-34-MM (full circles) and MnO_x+SAPO-34-SM (empty triangles). Reaction conditions: m(MnO_x)=270 mg, m(SAPO-34)=30 mg, P=25 bar, T=410 °C, $H_2/CO/N_2$=60/30/10, WHSV 87 $mL.min^{-1}.g^{-1}$.

Similar temporal evolution was also observed for the selectivity sets of the two mixtures, with a small increase in CH_4 and C2 selectivity, while the C3 and C4 selectivity slightly decreased (Figure 4b). Note that as expected for a SAPO-34 zeolite, the C2-C4 selectivity was high (ca 55% after 14 h). Furthermore, as shown in Table 1, the selectivity values after 14 h were close even if a slightly lower C2-C3 selectivity was obtained for MnO_x+SAPO-34-MM (49 vs 52%) to the benefit of the CH_4 one (12 vs 9%). This difference, more pronounced initially (Figure 4b), could be related to the difference of intimacy. Indeed, a lower proximity between the oxide and the zeolite grains should favor CH_3OH hydrogenation to CH_4.[5,8,9]

Table 1. X(CO) conversion and O/P ratio, CO_2, CH_4 and hydrocarbon selectivity for MnO_x+SAPO-34-MM and MnO_x+SAPO-34-SM. Reaction conditions: m(MnO_x) =270 mg, m(SAPO-34) =30 mg, P=25 bar, T=410 °C, $H_2/CO/N_2$=60/30/10, WHSV 87 $mL.min^{-1}.g^{-1}$. Data were taken after 14 h on stream.

		Selectivity (%)						
	X(CO) (%)	O/P	S(CH4)	S(CO2)	S(C2)	S(C3)	S(C4)	S(C5+)
MnOx-+SAPO-34-MM	4.1	16.2	12	33	24	25	4	2
MnOx +SAPO-34-SM	4.4	16.8	9	33	25	27	4	2

Figure 4a shows that the olefin to paraffin O/P ratio was initially higher for the SM catalyst than for the MM one (~10.0 vs 5.8). Furthermore, the evolutions were different: the O/P ratio reaches its maximum after 4 h for the SM and after 6 h for the MM sample. The O/P maximum reached for the SM (18.7), is higher than for the MM (16.6). Then, the two curves converge toward a similar value of O/P ~ 16, after 14 h on stream.

Those results suggest that the catalytic properties of the two catalyst mixtures, initially different, converge over time on stream. SEM images of the MM sample were recorded right after activation under H2 flow. Figure 5a shows the presence of well-defined zeolite aggregates of ca 100-200 µm size that are covered by MnO_x primary particles (see also the zoom in Figure S7a).

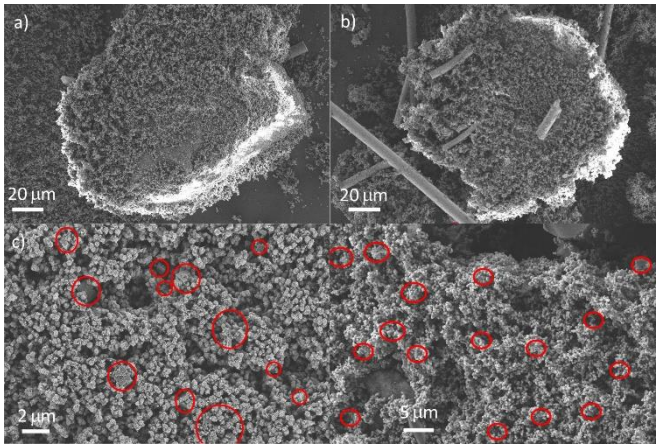

Figure 5. SEM images of 90%MnO_x+10%SAPO-34-MM after activation under 20 nml/min of H_2 at 430 °C for 4 h and (a) 0 h, (b) 2 h, (c) 14 h on stream and (d) SEM images of 90%MnO_x+10%SAPO-34-SM after activation under 20 nml/min of H_2 at 430 °C for 4 h and 14 h on stream. The needles in Figure 5b correspond to quart wool added to the catalytic bed. Reaction conditions: m(MnO_x) =270 mg, m(SAPO-34) =30 mg, P=25 bar, T=410 °C, H_2/CO/N_2=60/30/10, WHSV 87 $mL.min^{-1}.g^{-1}$.

Conversely, only few SAPO-34 crystals were distinguished among the primary MnO_x aggregates (Figure S7b). Hence, SEM analysis revealed that intimacy of the MnO_x+SAPO-34-MM mixture after activation was similar to that of the fresh state, with well-separated aggregates of MnO_x and SAPO-34 (Figure 6a).

SEM images were also recorded after 2 h on stream: large aggregates of zeolite are still visible in Figure 5b. However, they seem to begin to lose their shape as revealed by Figure 6b (in grey in Figure S8b): SAPO-34 crystals begin to separate from each other and the transition between zeolite and oxide domains is less sharp. Indeed, as shown in Figure S8a, more zeolite crystals are dispersed inside the MnO_x domains. However, large domains of zeolite with small quantity of MnO_x primary particles are still visible. Those images suggest that a textural evolution takes place under the reaction conditions on stream, improving the intimacy, and that it is a slow phenomenon.

Finally, SEM images were recorded after 14 h on stream for both mixtures. It appears that the intimacy of MnO_x+SAPO-34-MM greatly improved with time on stream: no zeolite aggregates are observed anymore, but only a homogeneous powder is visible at the 10 µm scale, Figure 5c. Figure 6c and Figure S9 clearly show that the powder is composed of SAPO-34 crystals well dispersed among the MnO_x agglomerates. Hence, a high intimacy was obtained for MnO_x+SAPO-34-MM, similar to fresh MnO_x+SAPO-34-SM. Note that the intimacy of this latter mixture does not evolve significantly under the reaction conditions: no specific aggregates could be identified while some SAPO-34 crystals were well dispersed in the MnO_x powder (Figures 5d, 6d and S10).

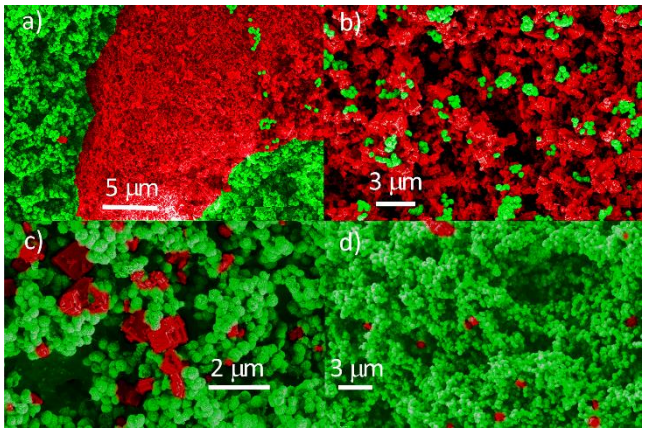

Figure 6. SEM images of 90%MnO_x+10%SAPO-34-MM (a) after activation under 20 nml.min-1 of H_2 at 430 °C for 4 h, b) after activation and 2 h on stream, (c) after activation and 14 h on stream and d) 90%MnO_x+10%SAPO-34-SM after activation under 20 nml.min^{-1} of H_2 at 430 °C for 4 h and 14 h on stream. SAPO-34 crystals are colored in red and MnO_x nanoparticles in green. Reaction conditions: m(MnO_x)=270 mg, m(SAPO-34)=30 mg, P=25 bar, T=410 °C, H_2/CO/N_2=60/30/10, WHSV 87 mL.min^{-1}.g^{-1}.

The early evolution of catalytic properties of OX-ZEO bifunctional catalysts is not really addressed in literature even if often noticeable.[2,8,24-26] It could arise from equilibration of diffusion processes occurring in the zeolite during formation of the hydrocarbon pool.[27] However, the olefin to paraffin O/P ratio was shown to strongly depend on the density of Brønsted acid sites (BAS) while the CO conversion is almost constant when the BAS density is high enough to convert CH_3OH.[8,28-30] Therefore, the temporal increase in the O/P ratio could arise from a decrease in the BAS density while remaining high enough to keep the conversion constant. Therefore, the difference of evolution between MM and SM catalysts has to be explained by the evolution of another parameter. One could assume that Mn^{2+} cations tend to migrate into the zeolite under the harsh reaction conditions of the OXZEO process as previously reported for other metals.[31] However, Ding et al. [7] who also studied MnO_x+SAPO-34 mixtures reported that such migration was negligible. Furthermore, Mn-exchanged SAPO-34 prepared by us, was poorly active (X(CO)=1%, Figure S12), showing that the two active sites for the conversion of syngas into light olefins are definitely the MnO_x surface and BAS of the SAPO-34 crystals.

It was previously reported that the distance between $ZnZrO_x$ oxide and zeolite does not influence the catalytic properties for the conversion of syngas to olefins, contrarily to syngas to aromatics process, because of fast diffusion of methanol.[32] In the present work, the temporal evolution of the O/P ratio could be partly related to the evolution of intimacy i.e. of the distance between the oxide and the zeolite. Indeed, its improvement probably decreases the diffusion path of methanol toward the zeolite and of the olefins outward it. However, the apparent syngas consumption rate is kinetically limited by the formation of methanol on the oxide and not by the diffusion of methanol inside the zeolite aggregates. Otherwise, the conversion should increase as a function of time on stream which is not observed experimentally. In a similar manner, because the oxide aggregates do not change in size under stream, the methanol diffusion flow inside of the oxide is not modified and the methane selectivity related to the oxide is almost not affected. On the other hand, the improvement of intimacy leads to a decrease in the contact time of the olefins with the zeolite. This helps to reduce the proportion of olefins that is converted into paraffins and hence to improve the O/P ratio. Ding et al. also observed an improvement of the O/P increasing proximity between MnO_x and SAPO-34 samples

with grains ranging from 900 to 200 µm. However, SAPO-34 aggregates kept their shape under stream unlike in this study.[7]

The fundamental driving force of the improvement of intimacy of 90%MnO_x+10%SAPO-34-MM is certainly entropy, that always favors a homogeneous mixture of (weakly interacting) particles over an inhomogeneous one. Apparently, soft agglomerates of zeolite are broken and redistributed under the reaction conditions. Then, the "driving forces" that provide input of energy and make the particles move are probably temperature and pressure (which allow to break the agglomerates) and microscopic fluctuations of gas flow (which allow displacing the particles). As a result, the static bed appears to be not-so-static, and this is one of the main points of our paper.

Conclusion

In this study, it was shown that the intimacy of a mechanical mixture composed of MnO_x and SAPO-34 agglomerates improves during the first hours in reaction conditions. During this period, agglomerates of SAPO-34 crystals are broken and their dispersion occurs among MnO_x primary particles. The increase of O/P ratio with time on stream is proposed to be partly related to this intimacy improvement. After 14 h, the intimacy reached was close to that obtained for a suspension mixture, leading to similar catalytic properties. It clearly shows that high intimacy at the micrometer scale is required to get high performances for the Ox-Zeo process and intimacy optimization is further needed.

Experimental Section

MnO_x powder was prepared from $MnCO_3$ as follows: two 0.5 M aqueous solutions of $(NH_4)_2CO_3$ (Alfa aesar, Ref 36229, NH3 30.0%) and $MnSO_4$ (Prolabo, Ref 25-301, 98%) were prepared. 5 ml of each solution were sampled and 6.35 ml of glycerol (Sigma-Aldrich, Ref G7893, 99.5%) were added to each of them and stirred until homogenization. The $(NH_4)_2CO_3$ solution was added to the $MnSO_4$ solution under stirring and left at room temperature under stirring for 1 h. Upon addition of the carbonate solution to the sulphate solution, a white suspension was formed. After 1 h of stirring, the suspension was centrifuged (3500 rpm) and washed three times with water. The recovered $MnCO_3$ solid was dried at 100 °C overnight. Then the obtained powder was treated under 20%H_2-N_2 flow of 100 mL. min^{-1} at 430 °C for 12 h to produce MnO particles. After the treatment, MnO was exposed to flowing air at room temperature to passivate the surface.

The preparation of SAPO-34 was carried out as follows: 16.8 g of Al-isopropoxide (Sigma Aldrich, 220418, ≥ 98%) and 39 ml of TEAOH (Alfa Aesar, 43023, 35 wt% in H2O) were mixed in a Teflon recipient for 1h30 at room temperature. After that, 0.74 g of silica (Evonik, Aerosil 200 153070413, ≥99.99%) was added to the mixture and mixed for 1 h. Finally, 9,4 g of H_3PO_4 (Honeywell Fluka, 30417-1L, ≥85%) and 8,7 g of H_2O were added to the mixture and stirred for 3 h at room temperature. Then the Teflon recipient was closed and placed in a stainless-steel autoclave which was heated to 100 °C for 12 h without stirring, for ageing. Finally, the autoclave was heated to 200 °C and maintained at this temperature for 48 h under autogenous pressure. After this step, the suspension was recovered and washed by water with repetitive centrifugation. The recovered solid was dried at 100 °C overnight and then calcined in air at 200 °C for 2 h (heating rate of 1 °C.min^{-1}). Then, the temperature was increased slowly up to 550 °C with a ramp of 0.5 °C.min^{-1} and maintained for 6 h.

To prepare the SM- sample, 143 mg of calcined SAPO-34 was finely grinded, added to 5 ml of ethanol and stirred vigorously. The obtained suspension was then treated in an ultrasound bath for 15 min to favour dispersion of particles. A $MnCO_3$ suspension was prepared as previously described for MnO_x. After washing, 1.700 g of $MnCO_3$ nanoparticles were re-dispersed in 50 ml of ethanol passed in an ultrasound bath for 15 min producing a suspension. Then, the two suspensions were mixed together

and dried at 100 °C over day. It would lead after calcination to a mixture composed of 1.050 g of MnO_x and 0.143 g of SAPO-34 (12% of zeolite). During the drying step, the suspension was periodically shacked at 30 min interval to ensure that no segregation between the SAPO-34 and $MnCO_3$ particles occurred. After drying, the obtained powder was treated thermally under 20%H_2-N_2 at 430 °C for 12 h. The resulting solid is named 90%MnO_x+10%SAPO-34-SM in the manuscript. By comparison, 90%MnO_x+10%SAPO-34-MM was a mechanical mixture of 90 wt% of MnO_x and 10 wt% of SAPO-34, separately sieved between 180 µm and 105 µm.

Inductively Coupled Plasma-Optical Emission Spectrometry (ICP-OES) has been used for quantification of Si, Al, P and Mn on an ICP-OES Activa spectrometer (Horiba). For Al, P and Mn quantification, the solid was firstly dissolved in H_2SO_4+HNO_3+HF at boiling point before being injected into the analysis apparatus. For Si, the solid has been fused with lithium tetraborate into a Pt-Au crucible at 1100 °C. The obtained solid was then dissolved into a 20% HCl solution before injection.

X-ray diffractograms were obtained between 4 and 80° (2Θ) on a Bruker D8 Advance A25 diffractometer equipped with a Ni filter (Cu Kα radiation: 0.154184 nm) and a one-dimensional multistrip detector (Lynxeye, 192 channels on 2.95°). The counting time per point was 0.5 s. The International Center for Diffraction Data (ICDD) library was used for phase identification. Furthermore, the crystallite size was determined using the Scherrer equation: $D=K\lambda/(\beta i*\cos(\theta))$ where D is the crystallite size, λ the wavelength of the X-ray beam, βi the full width half maximum corrected of the instrumental width (0.06°) and θ the diffraction peak angle.

Transmission electron microscopy (TEM) images were acquired using a JEOL 2010 with a 200 kV accelerating voltage equipped with a LaB6 source and a CCD Gatan camera. The spatial resolution was 0.19 nm. The TEM device was coupled with energy dispersive (EDS) spectrometer (Oxford Instruments).

Scanning electron microscopy (SEM) analyses have been used to follow the textural evolution of the catalyst mixture after activation and after catalytic test. SEM images were recorded on a Zeiss Merlin Compact, using the secondary electron detector and an acceleration voltage of 5 kV. Elemental composition was probed by switching the accelerating voltage to 15 kV and using the EDX (energy dispersive X-Ray) detector.

Textural analyses of MnOx oxides and SAPO-34 zeolites were performed by N_2 physisorption at -196 °C on a micromeritic ASAP 2020 instrument after desorption of the solid at 400 °C for 2 h under vacuum of 0.1 Pa. The BET method was used to determine the BET surface area, the BJH method to determine the pore volume and size and the t-plot method to determine microporosity.

NH_3-TPD measurements were performed to determine the quantity and strength of acid sites of SAPO-34 using a BelCat-M (Bel Japan Inc.) apparatus equipped with a TCD detector. First around 60 mg of solid was flushed under He flow at 400 °C for 1 h to remove adsorbed molecules and the solid was exposed to 50 nml.min^{-1} of 1% NH_3-He for 30 min. After flushing the sample under He at 100 °C until a stable TCD signal was observed, the temperature was raised at a rate of 10 °C/min under 50 nmL.min^{-1} of He. The number of acid sites was determined by integration over time of the quantity of NH_3 desorbed.

Catalytic testing has been performed with a home-made apparatus containing the reaction and pre-treatment gas inlet lines of CO, H_2 and N_2. Each line was composed of a Brooks 5850 TR flow regulator, a manometer and a stop valve. A straight tubular steel reactor (internal diameter of 6 mm) containing powder samples and heated with a tubular furnace was used. A thermowell with an external diameter of 1.6 mm passed through the whole reactor allowing temperature measurement across the whole

catalytic bed which was centered in the reactor using quartz wool. The gas at the outlet of the reactor was flowing either to a vent or to a manual pressure regulator. All the lines after the reactor were heated at 100 °C to avoid condensation of liquid products. The gas analysis has been performed at atmospheric pressure with two microGC chromatographs equipped with a TCD detector: the first one contained a molecular sieve and an alumina Na2SO4 column for separation of CO, H_2, CH_4 and N_2 and of C2 to C6 hydrocarbons, respectively. The second one (3000/Inficon) was equipped with a Plot-U-column for analysis of CO_2. The carbon balance was 100 ±5 %.

The catalyst was activated at atmospheric pressure 20%H_2-N_2 at 430 °C for 4 h. Then, the reactor was flushed under N_2, the pressure increased to 25 bars and the temperature set to 410 °C. The reactants were preloaded in their respective inlet lines to 25 bars before setting the flow rates and opening the inlet valves. Usually, the catalytic measurements lasted for at least 14 h to reach an apparent steady state.

Acknowledgements

The French National Research agency 'Agence Nationale de la Recherche' (ANR) is acknowledged for the financial support of the INCH project (ANR-17-CE07-0011).

Keywords: syngas • light olefins • OXZEO process• intimacy • in situ textural evolution

References

[1] M. Monai, M. Gambino, S. Wannakao, B.M. Weckhuysen, Chem. Soc. Rev. 2021, 50, 11503–11529.

[2] F. Jiao, J. Li, X. Pan, J. Xiao, H. Li, H. Ma, M. Wei, Y. Pan, Z. Zhou, M. Li, S. Miao, J. Li, Y. Zhu, D. Xiao, T. He, J. Yang, F. Qi, Q. Fu, X. Bao, Science 2016, 351, 1065–1068.

[3] W. Zhou, K. Cheng, J. Kang, C. Zhou, V. Subramanian, Q. Zhang, Y. Wang, Chem. Soc. Rev. 2019, 48, 3193–3228.

[4] X. Pan, F. Jiao, D. Miao, X. Bao, Chem. Rev. 2021, 121, 11, 6588–6609.

[5] C. Coudercy, V. L'hospital, R. Checa, A. Le Valant, P. Afanasiev, S. Loridant, Catal. Sci. Technol. 2021,11, 7844–7849.

[6] H. Jiang, Z. Hou, Y. Luo, ACS Catal. 2020, 10, 13518−13523.

[7] Y. Ding, F. Jiao, X. Pan, Y. Ji, M. Li, R. Si, Y. Pan, G. Hou, X. Bao, ACS Catal. 2021, 11, 9729–9737.

[8] X. Liu, W. Zhou, Y. Yang, K. Cheng, J. Kang, L. Zhang, G. Zhang, X. Min, Q. Zhang, Y. Wang, Chem. Sci. 2018, 9, 4708–4718.

[9] K. Cheng, B. Gu, X. Liu, J. Kang, Q. Zhang, Y. Wang, Angew. Chem. Int. Ed. 2016, 55, 4725–4728.

[10] P. Gao, S. Li, X. Bu, S. Dang, Z. Liu, H. Wang, L. Zhong, M. Qiu, C. Yang, J. Cai, W. Wei; Y. Sun, Nature Chem. 2017, 9, 1019–1024.

[11] C. Kosanovic, J. Bronic, B. Subotic, I. Smit, M. Stubicar, A. Tonejc, T. Yamamoto, Zeolites 1993, 13, 261–268.

[12] C. Kosanovic, J. Bronic, A. Cizmek, B. Subotic, I. Smit, M. Stubicar, A. Tonejc, Zeolites 1995, 15, 247–252.

[13] Saepurahman, R. Hashaikeh, Mater. Chem. Phys. 2018, 220, 322–330.

[14] M. T. Buscaglia, M. Bassoli, V. Buscaglia, R. Alessio, J. Am. Ceram. Soc. 2005, 88, 2374–237 9.

[15] M. T. Buscaglia, M. Bassoli, V. Buscaglia, R. Vormberg, J. Am. Ceram. Soc. 2008, 91, 2862–2869.

[16] S. D. Škapin, V. Čadež, D. Suvorov, I. Sondi, J. Colloid and Interface Sci. 2015, 457, 35–42.

[17] Y. Zeng, L. Prasetyo, S. J. Tan, C. Fan, D. D. Do, D. Nicholson. Chem. Eng. Sci. 2017, 158, 462–479.

[18] Z. Wang, X. Jiang, M. Pan, Y. Shi, Minerals 2020, 10, 377.

[19] K. A. Cychosz, M. Thommes, M. Engineering 2018, 4, 559–566.

[20] R. Vomscheid, M. Briend, M. J. Peltre, P. Massiani, P. P. Man, D. Barthomeuf, J. Chem. Soc., Chem. Commun. 1993, 6, 544.

[21] M. E. Potter, M. E. Down ACS Catal. 2020, 10, 9758–9789.

[22] W. Shen, X. Li, Y. Wei, P. Tian, F. Deng, X. Han, X. Bao, Micropor. Mesopor. Mat. 2012, 158, 19–25.

[23] A. Buchholz, W. Wang, M. Xu, A. Arnold, M. Hunger, Micropor. Mesopor. Mat. 2002, 56, 267–278.

[24] J. Su, H. Zhou, S. Liu, C. Wang, W. Jiao, Y. Wang, C. Liu, Y. Ye, L. Zhang, Y. Zhao, H. Liu, D. Wang, W. Yang, Z. Xie, M. He, Nature Commun. 2019, 10, 1297.

[25] N. Li, F. Jiao, X. Pan, Y Ding, J. Feng, X. Bao, ACS Catal. 2019, 9, 960–966.

[26] F. Meng, X. Li, P. Zhang, L. Yang, G. Yang, P. Ma, Z. Li, Catal. Today 2021, 368, 118–125.

[27] N. Nesterenko, J. Aguilhon, Ph. Bodart, D. Minoux, J.-P. Dath, in Zeolites and Zeolite-Like Materials, 1 st Edition (Eds: Bert F. Sels and Leonid M. Kustov), Elsevier, 2016, Ch.5.

[28] M Wang, Z. Wang, S. Liu, R. Gao, K. Cheng, L. Zhang, G. Zhang, X. Min, J Kang, Q. Zhang, Y. Wang, J Catal. 2021, 394, 181–192.

[29] X. Liu, M. Wang, H. Yin, J. Hu, K. Cheng, J. Kang, Q. Zhang, Y. Wang, ACS Catal. 2020, 10, 8303−8314.

[30] G. Li, F. Jiao, X. Pan, N. Li, D. Miao, L. Li, X. Bao, ACS Catal. 2020, 10, 12370−12375.

[31] Y. Wang, G. Wang, L. I. van der Wal, K. Cheng, Q. Zhang, K. P. de Jong, Y. Wang, Angew. Chem. Int. Ed. 2021, 60, 17735−17743.

[32] Y. Li, M. Wang, S. Liu, F. Wu, Q. Zhang, S. Zhang, K. Cheng, Y. Wang, ACS Catal. 2022, 12, 8793−8801.

Entry for the Table of Contents

In situ generation of intimacy during the OXZEO process

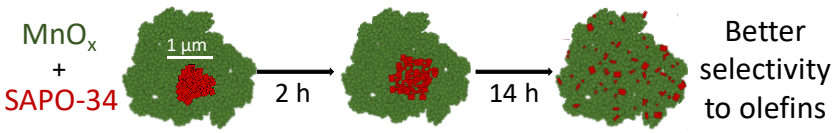

The intimacy of a mechanical mixture composed of MnO_x and SAPO-34 agglomerates improves during the conversion of syngas into light olefins. Such in situ generation of intimacy led to high dispersion of SAPO-34 crystals among MnO_x primary particles as obtained for fresh MnO_x and SAPO-34 suspension mixture and could explain convergence of the catalytic properties after 14 h on stream.